



ARTICLE

# A Dynamical Study of Modeling the Transmission of Typhoid Fever through Delayed Strategies

Muhammad Tashfeen<sup>1</sup>, Fazal Dayan<sup>1</sup>, Muhammad Aziz Ur Rehman<sup>1</sup>, Thabet Abdeljawad<sup>2,3,4,5,\*</sup> and Aiman Mukheimer<sup>2</sup>

<sup>1</sup>Department of Mathematics, School of Science, University of Management and Technology, Lahore, 54000, Pakistan

<sup>2</sup>Department of Mathematics and Sciences, Prince Sultan University, P.O. Box 66833, Riyadh, 11586, Saudi Arabia

<sup>3</sup>Department of Medical Research, China Medical University, Taichung, 40402, Taiwan

<sup>4</sup>Department of Mathematics and Applied Mathematics, School of Science and Technology, Sefako, Makgatho Health Sciences University, Ga-Rankuwa, 0208, South Africa

<sup>5</sup>Center for Applied Mathematics and Bioinformatics (CAMB), Gulf University for Science and Technology, Hawally, 32093, Kuwait

\*Corresponding Author: Thabet Abdeljawad. Email: tabeljawad@psu.edu.sa

Received: 28 April 2024 Accepted: 28 July 2024 Published: 27 September 2024

## ABSTRACT

This study analyzes the transmission of typhoid fever caused by *Salmonella typhi* using a mathematical model that highlights the significance of delay in its effectiveness. Time delays can affect the nature of patterns and slow down the emergence of patterns in infected population density. The analyzed model is expanded with the equilibrium analysis, reproduction number, and stability analysis. This study aims to establish and explore the non-standard finite difference (NSFD) scheme for the typhoid fever virus transmission model with a time delay. In addition, the forward Euler method and Runge-Kutta method of order 4 (RK-4) are also applied in the present research. Some significant properties, such as convergence, positivity, boundedness, and consistency, are explored, and the proposed scheme preserves all the mentioned properties. The theoretical validation is conducted on how NSFD outperforms other methods in emulating key aspects of the continuous model, such as positive solution, stability, and equilibrium about delay. Hence, the above analysis also shows some of the limitations of the conventional finite difference methods, such as forward Euler and RK-4 in simulating such critical behaviors. This becomes more apparent when using larger steps. This indicated that NSFD is beneficial in identifying the essential characteristics of the continuous model with higher accuracy than the traditional approaches.

## KEYWORDS

Typhoid virus; delay epidemic model; stability; consistency; global stability

## 1 Introduction

Infectious diseases can be transmitted directly or indirectly between individuals. These illnesses emerge when microorganisms enter the body, increase, and trigger a resistant reaction. Typhoid fever, whenever left untreated, represents a severe gamble, possibly harming various organs and prompting



deadly entanglements. It is brought about by *Salmonella Typhi* [1], frequently present in sullied food or water. Ingesting sullied substances presents the microorganisms, causing sickness. Notwithstanding upgrades in water neatness, typhoid fever remains a critical worry in many non-industrial countries [2]. Normal side effects incorporate migraines, queasiness, heaving, looseness of the bowels, rashes, fever, joint and muscle torment, and loss of hunger. Untreated, it can rise, influencing the bloodstream and causing stomach tissue contamination [3]. Numerical models have played a crucial role in disentangling typhoid fever's transmission components and assessing the viability of preventive measures. Although some explicitly tackle direct human-to-human transmission [4–6], others additionally consider the job of debased food and water in aberrant transmission [7–9].

Far-reaching models have provided a more profound comprehension by investigating both immediate and roundabout transmission methods [10–12]. These models have fundamentally supported evaluating intercessions, for example, sickness therapy [13,14], sterilization rehearsal [15,16], instructive missions [17], and media drives [18] pointed toward forestalling typhoid flare-ups. Their bits of knowledge are instrumental in contriving effective control measures for typhoid fever. For example, Musa et al. [19] fostered a plague model to investigate typhoid fever transmission and evaluate the effect of general Wellbeing instruction crusades on bringing down infection rates. Using information from Taiwan and China, they adjusted the model, laying out security measures for endemic and illness-free harmony. Utilizing wavelet examination, they distinguished urgent occasional examples in episodes and decided critical boundaries for typhoid disease the executives. Peter et al. [20] introduced a numerical model to investigate typhoid transmission elements and the impacts of immunization, incorporating immediate and circuitous effects, like group invulnerability. They showed that while inoculation could briefly offer backhanded assurance and decrease sickness occurrence, destroying Typhoid exclusively through immunization appeared to be unrealistic. Edward et al. [21] created a numerical model thinking about both immediate and backhanded transmissions of typhoid fever. They assessed medications such as treatment, inoculation inclusion, and water disinfection. They focused on the significance of restricting contact with typhoid patients and forestalling water pollution with fertilizer as the essential strategies to stop typhoid scourges. Inside the range of enteritis problems, typhoid fever remains a common irresistible sickness set off by *Salmonella Typhi* microorganisms in the human body.

This sickness normally spreads through sullied food and water corrupted by a contaminated person's dung or pee [22]. It is remarkably more pervasive in immature locales because of unfortunate food disinfection, debased water sources, and deficient ecological cleanliness. Side effects manifest during the seven to fourteen-day hatching period and incorporate migraines, stomach inconvenience, joint and back torments, muscle throbs, decreased craving, retching, runs, rashes, and fever [23–25]. According to the World Wellbeing Association's assessments, Typhoid fever generally represents 0.6 million passings and 17 million cases annually [26]. Over the past two decades, numerous studies have resulted in the development of diverse mathematical models. For instance, a model is formulated featuring four compartments: susceptible, infected, asymptomatic carriers, and recovered individuals [27,28].

Delay in mathematical epidemic models refers to the time it takes for an individual to become infectious after being infected. This delay is crucial in understanding the spread of diseases and is incorporated into models through time-delay differential equations. Based on the most recent research, time delays favorably impact the dynamics of epidemic models by influencing time delay pattern creation and the emergence of variational patterns, as well as guiding the spectrum of dynamical phenomena of epidemic models. Time delay plays an important part in modeling numerous aspects of disease transmission, such as the quarantine period in an infectious condition, which provides a

more valuable portrayal of epidemic scenarios [29–31]. Time delays are advantageous in epidemics by emphasizing patterns and their dynamic analysis, executing model findings and regulating techniques for the distinct management of illness, and providing a thorough grasp of disease propagation dynamics compared to older models. Many new researchers have a remarkable insight that favors the application of delay differential equations in epidemics modeling. Delay dynamics in transmission rates can aid in anticipating the transmission rates of disease spread and control measures. In addition, delays can be considered for the intervention and majorly impact regulating tactics. These findings highlighted the importance of including delays in mathematical epidemic models to improve prediction behavior and assist public health decision-making [32]. Goel et al. [33] studied a new nonlinear time delay SIR (Susceptible-Infectious-Recovered) model with a Beddington-DeAngelis incidence rate, and Hill's functional-type saturated recovery rate was developed to study the epidemic control, which further contributed to the development of a two-strain epidemic model considered the distributed recovery and death rates and involving delay equations.

Compared to standard models, epidemic models with delays provide a more practical knowledge of disease dynamics by encompassing the temporal components of transmission and control methods. Ghosh et al. [34] highlighted that time delay can improve time lags on epidemic outcomes, evaluate the effectiveness of control strategies, and optimize resource allocation in mathematical epidemic models present infectious disease, allowing for more accurate examination of epidemic risk and assisting in taking precautions for public health. The NSFD scheme is employed to obtain reliable solutions in delayed stochastic and fuzzy extensions [35–39], to mention a few. Cheng et al. [40] developed and examined a network-based SIQS (susceptible-infected-quarantined-susceptible) infectious disease model featuring a nonmonotone incidence rate. The basic reproduction number and the equilibria of the model are determined analytically, global stability is explored, and numerical simulations are conducted to support the theoretical findings.

This study aims to increase the reliability of the mathematical models of typhoid fever transmission by including time delays in the equation because they strongly affect the trends of the infection. This kind of modeling can enhance prediction and public health efforts to tackle typhoid fever outbreaks. The SEIRS (Susceptible-Exposed-Infectious-Recovered-Susceptible) model and the SEIRS delay model are made up of the same structural parts, but the time delay function distinguishes them. In its baseline model, SEIRS makes no provision for delays; rather, compartments Susceptible, Exposed, Infectious, Recovered, and Susceptible are described by ODEs (ordinary differential equation) that do not include time delays when an individual shifts from the former compartment to the latter one or vice versa. However, the SEIRS delay model introduces the concept of delay using DDEs (delayed differential equation) to capture a given incubation period and other temporal delays better than the basic SEIRS model. This addition enhances projection performance for disease type with a long latency time and enhances computational calculation. The delay Susceptible-Exposed-Infectious-Recovered (SEIR) model is a better version that demonstrates how the diseases progress over time and can deliver more specifics for implementing a plan to prevent the spread of diseases. The novelty of the proposed approach is the construction, implementation, and analysis of a first-order explicit numerical scheme in non-standard finite difference settings for Typhoid fever with time delay.

This research looks at several aspects of Typhoid virus transmission among communities. [Section 2](#) offers a mathematical model that depicts the dynamics of the propagation. This section addresses the virus's reproductive characteristics and immediate transmission without delay. It also investigates the existence of endemic equilibrium and evaluates its local stability. [Section 3](#) contains the delayed epidemic model and conducts a stability analysis considering delays. [Sections 4](#) and [5](#) are dedicated to presenting mathematical modeling and numerical simulations that validate the outcomes

of our proposed system to corroborate the results obtained. Sections 6 and 7 contain parameter estimation analysis and conclusions, respectively.

### 2 Modified SEIR Epidemic Model

The system of differential equations derived from [41] is

$$\begin{cases} \frac{dS}{dt} = \alpha - \beta SI + \omega R - \mu S, \\ \frac{dE}{dt} = \beta SI - \varphi E - \mu E, \\ \frac{dI}{dt} = \varphi E - \sigma I - \delta I - \mu I, \\ \frac{dR}{dt} = \sigma I - \omega R - \mu R. \end{cases} \tag{1}$$

These factors are inherent in an epidemiological model, frequently associated with the SEIR model used in disease transmission research. Within this approach,  $S$  symbolizes the susceptible population that has not yet been impacted by the disease, whereas  $E$  represents the exposed population of individuals who have been exposed to the disease but are not yet contagious.  $I$  indicates people actively infected and spreading the disease, whereas  $R$  represents those who have recovered and gained immunity. The symbol  $\alpha$  reflects the recruiting rate, indicating new people joining the vulnerable group.  $\mu$  represents the post-infection mortality rate, whereas  $\beta$  represents infection rates among vulnerable individuals.  $\varphi$  denotes the rate of transition from exposed to infected,  $\sigma$  denotes the rate of transition from infected to recovered,  $\delta$  represents post-infection mortality rate. Finally,  $\omega$  reflects the rate of change from recovered to susceptible, which may indicate diminishing immunity or susceptibility to reinfection. These factors are critical in mathematical models for simulating disease transmission patterns and forecasting population outbreaks. This study added the concept of susceptibility to the improved SEIRS epidemic model. The rate indicates that individuals who recovered will transition back to the susceptible group after being infectious. This explains why they are less likely to develop the same infection again. The flowchart of the model is shown in Fig. 1.

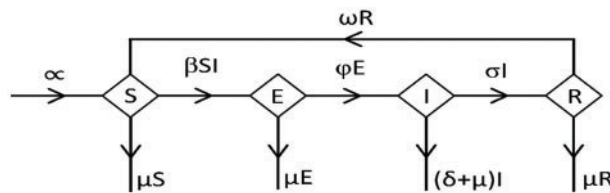


Figure 1: Flowchart of the model

#### 2.1 The Basic Reproductive Number (BRN)

Let  $X = (E, I)'$  then  $\frac{dx}{dt} = \mathcal{F}(x) - \Delta(x)$  and  $\mathcal{F}(x) = \begin{bmatrix} \beta SI \\ 0 \end{bmatrix}$ ,  $\Delta(x) = \begin{bmatrix} (\varphi + \mu)E \\ -\varphi E + (\sigma + \delta + \mu)I \end{bmatrix}$ . Further,  $\mathcal{F}$  and  $\Delta$  are the Jacobians of  $\mathcal{F}(x)$  and  $\Delta(x)$  respectively at disease-free equilibrium point  $E^{d_1}(S^0, E^0, I^0, R^0) = \left(\frac{\alpha}{\mu}, 0, 0, 0\right)$  and are given as follows:

$$\mathcal{F} = \begin{bmatrix} 0 & \frac{\beta \alpha}{\mu} \\ 0 & 0 \end{bmatrix}, \Delta = \begin{bmatrix} (\varphi + \mu) & 0 \\ -\varphi & (\sigma + \delta + \mu) \end{bmatrix}.$$

Now

$$\mathcal{T} = \mathcal{F}\Delta^{-1} = \begin{bmatrix} 0 & \frac{\beta \alpha}{\mu(\varphi + \mu)} \\ 0 & \frac{\beta \varphi \alpha}{\mu(\varphi + \mu)(\sigma + \delta + \mu)} \end{bmatrix}.$$

The spectral radius of  $\mathcal{F}\Delta^{-1}$  is

$$\rho(\mathcal{F}\Delta^{-1}) = \frac{\beta \varphi \alpha}{\mu(\varphi + \mu)(\sigma + \delta + \mu)}$$

The BRN  $\mathcal{R}_o$  is given by

$$\mathcal{R}_o = \frac{\beta \varphi \alpha}{\mu(\varphi + \mu)(\sigma + \delta + \mu)}. \tag{2}$$

### 2.2 Equilibrium Analysis

The system (1) has a disease-free equilibrium (DFE) point  $E^1(S^o, E^o, I^o, R^o) = \left(\frac{\alpha}{\mu}, 0, 0, 0\right)$  and an endemic equilibrium point  $E^2(S^*, E^*, I^*, R^*)$ , where

$$S^* = \frac{\alpha}{\mu \mathcal{R}_o},$$

$$E^* = \frac{k_3(\mu \alpha (1 - \mathcal{R}_o) k_3)}{\varphi(\mu \omega \mathcal{R}_o - \beta \alpha k_3)},$$

$$I^* = \frac{\mu \alpha (1 - \mathcal{R}_o) k_3}{\mu \omega \mathcal{R}_o - \beta \alpha k_3},$$

$$R^* = \frac{\sigma(\mu \alpha (1 - \mathcal{R}_o))}{\mu \omega \mathcal{R}_o - \beta \alpha k_3}, \text{ where } k_1 = (\varphi + \mu), k_2 = (\sigma + \delta + \mu) \text{ and } k_3 = (\mu + \omega).$$

### 2.3 Stability of Modified SEIR Model

The local stability of the modified SIER model is performed at  $E^1(S^o, E^o, I^o, R^o) = \left(\frac{\alpha}{\mu}, 0, 0, 0\right)$ . The eigenvalues of the system are  $\lambda_1 = -0.9000$ ,  $\lambda_2 = -0.9500$ ,  $\lambda_3 = -2.8248$ , and  $\lambda_4 = -0.4252$ . As all the eigenvalues are less than zero, it concluded that the system of differential equations of the SEIR model is locally asymptotically stable.

### 3 SEIR Model Modified with Time Delay

This section introduces a time delay parameter  $\tau$ .

### 3.1 Delay Differential Equation Model

Incorporating the impact of time delay in infected populations, model (1) assumes the following structure:

$$\begin{cases} \frac{dS}{dt} = \alpha - \beta SI + \omega R - \mu S, \\ \frac{dE}{dt} = \beta S(t - \tau)I(t - \tau)e^{-\mu\tau} - \varphi E - \mu E, \\ \frac{dI}{dt} = \varphi E - \sigma I - \delta I - \mu I, \\ \frac{dR}{dt} = \sigma I - \omega R - \mu R. \end{cases} \quad (3)$$

The symbol  $\tau$  is the latency period, indicating how long it takes for infected individuals to reach a contagious state, thus contributing to the ongoing spread of the virus. Within system (3), the expression  $\beta S(t - \tau)I(t - \tau)e^{-\mu\tau}$  at time ' $t$ ' reflects the transition of susceptible individuals to the infected group. The presence of  $e^{-\mu\tau}$  stems from presuming that population decline follows a linear pattern governed by  $\mu\tau$ , signifying the decrease in population during that specific duration due to factors like mortality or recovery.

### 3.2 The Basic Reproductive Number of Delayed Epidemic Model

Let  $X = (E, I)^t$  then  $\frac{dx}{dt} = \mathcal{F}(x) - \Delta(x)$  and  $\mathcal{F}(x) = \begin{bmatrix} \beta SIe^{-\mu\tau} \\ 0 \end{bmatrix}$ ,  $\Delta(x) = \begin{bmatrix} (\varphi + \mu)E \\ -\varphi E + (\sigma + \delta + \mu)I \end{bmatrix}$ . Further,  $\mathcal{F}$  and  $\Delta$  are now the Jacobians of  $\mathcal{F}(x)$  and  $\Delta(x)$  respectively at disease-free equilibrium point  $E^{d1} (S', E', I', R') = \left(\frac{\alpha}{\mu}, 0, 0, 0\right)$  such that

$$\mathcal{F} = \begin{bmatrix} 0 & \frac{\beta \alpha e^{-\mu\tau}}{\mu} \\ 0 & 0 \end{bmatrix}, \quad \Delta = \begin{bmatrix} (\varphi + \mu) & 0 \\ -\varphi & (\sigma + \delta + \mu) \end{bmatrix}.$$

Now,

$$\mathbb{T} = \mathcal{F}\Delta^{-1} = \begin{bmatrix} 0 & \frac{\beta \alpha e^{-\mu\tau}}{\mu(\varphi + \mu)} \\ 0 & \frac{\beta \varphi \alpha e^{-\mu\tau}}{\mu(\varphi + \mu)(\sigma + \delta + \mu)} \end{bmatrix}.$$

The spectral radius of  $\mathcal{F}\Delta^{-1}$  is

$$\rho(\mathcal{F}\Delta^{-1}) = \frac{\beta \varphi \alpha e^{-\mu\tau}}{\mu(\varphi + \mu)(\sigma + \delta + \mu)}$$

The BRN of the delayed epidemic model  $\mathcal{R}_{do}$  is given by

$$\mathcal{R}_{do} = \frac{\varphi \alpha \beta e^{-\mu\tau}}{\mu(\varphi + \mu)(\sigma + \delta + \mu)} \quad (4)$$

### 3.3 Equilibrium Analysis

The system (3) has a disease-free equilibrium point  $E^{d1} (S', E', I', R') = \left(\frac{\alpha}{\mu}, 0, 0, 0\right)$  and an endemic equilibrium point  $E^{d2} (S'', E'', I'', R'')$ , where

$$S'' = \frac{\alpha}{\mu \mathcal{R}_{do}},$$

$$E'' = \frac{k_3(\mu \alpha (1 - \mathcal{R}_{do}) k_3)}{\varphi(\mu \omega \mathcal{R}_{do} - \beta \alpha k_3)},$$

$$I'' = \frac{\mu \alpha (1 - \mathcal{R}_{do}) k_3}{\mu \omega \mathcal{R}_{do} - \beta \alpha k_3},$$

$$R'' = \frac{\sigma(\mu \alpha (1 - \mathcal{R}_{do}))}{\mu \omega \mathcal{R}_{do} - \beta \alpha k_3}, \text{ where } k_1 = (\varphi + \mu), k_2 = (\sigma + \delta + \mu) \text{ and } k_3 = (\mu + \omega).$$

### 3.4 Stability of Modified SEIR Delayed Model

The local stability of the modified SIER model is performed at  $E^{d1} (S', E', I', R') = \left(\frac{\alpha}{\mu}, 0, 0, 0\right)$ . The eigenvalues of the system are;  $\lambda_1 = -0.9000$ ,  $\lambda_2 = -0.9500$ ,  $\lambda_3 = -2.2412$  and  $\lambda_4 = -1.0088$ . As all the eigenvalues are less than zero, it concluded that the system of differential equations of the SEIR model is locally asymptotically stable.

## 4 Numerical Computation of Delayed Epidemic Model

### 4.1 Forward Euler's Method

The forward Euler scheme utilized for the model under study method involves making the following supposition can be expressed as follows:

Suppositions:  $S(t) \approx S^n$ ,  $S(t - \tau) \approx S_{n-m}$ ,  $I(t) \approx I^n$  and  $I(t - \tau) \approx I_{n-m}$ .

$$S^{n+1} = S^n + h[\alpha - \beta S^n I^n + \omega R^n - \mu S^n], \tag{5}$$

$$E^{n+1} = E^n + h[\beta S_{n-m} I_{n-m} e^{-\mu \tau} - (\varphi + \mu) E^n], \tag{6}$$

$$I^{n+1} = I^n + h[\varphi E^n - (\sigma + \delta + \mu) I^n], \tag{7}$$

$$R^{n+1} = R^n + h[\sigma I^n - (\mu + \omega) R^n]. \tag{8}$$

### 4.2 Fourth Order Runge Kutta Scheme (RK-4)

Considering the equations of system (3), the study develops an explicit RK-4 method. A numerical scheme for the RK-4 method is constructed as follows:

#### Step 1

$$k_1 = h[\alpha - \beta S^n I^n + \omega R^n - \mu S^n], \tag{9}$$

$$l_1 = h[\beta S_{n-m} I_{n-m} e^{-\mu\tau} - (\varphi + \mu) E^n], \quad (10)$$

$$p_1 = h[\varphi E^n - (\sigma + \delta + \mu) I^n], \quad (11)$$

$$m_1 = h[\sigma I^n - (\mu + \omega) R^n]. \quad (12)$$

**Step 2**

$$k_2 = h\left[\alpha - \beta\left(S^n + \frac{k_1}{2}\right)\left(I^n + \frac{p_1}{2}\right) + \omega\left(R^n + \frac{m_1}{2}\right) - \mu\left(S^n + \frac{k_1}{2}\right)\right], \quad (13)$$

$$l_2 = h\left[\beta\left(S_{n-m} + \frac{k_1}{2}\right)\left(I_{n-m} + \frac{p_1}{2}\right)e^{-\mu\tau} - (\varphi + \mu)\left(E^n + \frac{l_1}{2}\right)\right], \quad (14)$$

$$p_2 = h\left[\varphi\left(E^n + \frac{l_1}{2}\right) - (\sigma + \delta + \mu)\left(I^n + \frac{p_1}{2}\right)\right], \quad (15)$$

$$m_2 = h\left[\sigma\left(I^n + \frac{p_1}{2}\right) - (\mu + \omega)\left(R^n + \frac{m_1}{2}\right)\right]. \quad (16)$$

**Step 3**

$$k_3 = h\left[\alpha - \beta\left(S^n + \frac{k_2}{2}\right)\left(I^n + \frac{p_2}{2}\right) + \omega\left(R^n + \frac{m_2}{2}\right) - \mu\left(S^n + \frac{k_2}{2}\right)\right], \quad (17)$$

$$l_3 = h\left[\beta\left(S_{n-m} + \frac{k_2}{2}\right)\left(I_{n-m} + \frac{p_2}{2}\right)e^{-\mu\tau} - (\varphi + \mu)\left(E^n + \frac{l_2}{2}\right)\right], \quad (18)$$

$$p_3 = h\left[\varphi\left(E^n + \frac{l_2}{2}\right) - (\sigma + \delta + \mu)\left(I^n + \frac{p_2}{2}\right)\right], \quad (19)$$

$$m_3 = h\left[\sigma\left(I^n + \frac{p_2}{2}\right) - (\mu + \omega)\left(R^n + \frac{m_2}{2}\right)\right]. \quad (20)$$

**Step 4**

$$k_4 = h[\alpha - \beta(S^n + k_3)(I^n + p_3) + \omega(R^n + m_3) - \mu(S^n + k_3)], \quad (21)$$

$$l_4 = h[\beta(S_{n-m} + k_3)(I_{n-m} + p_3)e^{-\mu\tau} - (\varphi + \mu)(E^n + l_3)], \quad (22)$$

$$p_4 = h[\varphi(E^n + l_3) - (\sigma + \delta + \mu)(I^n + p_3)], \quad (23)$$

$$m_4 = h[\sigma(I^n + p_3) - (\mu + \omega)(R^n + m_3)]. \quad (24)$$

**Final Step**

$$S^{n+1} = S^n + \frac{1}{6}[k_1 + 2k_2 + 2k_3 + k_4], \quad (25)$$

$$E^{n+1} = E^n + \frac{1}{6}[l_1 + 2l_2 + 2l_3 + l_4], \quad (26)$$



$$I^{n+1} = I^n + \frac{1}{6} [p_1 + 2p_2 + 2p_3 + p_4], \tag{27}$$

$$R^{n+1} = R^n + \frac{1}{6} [m_1 + 2m_2 + 2m_3 + m_4]. \tag{28}$$

### 4.3 Non-Standard Finite Difference (NSFD) Scheme

The NSFD approach corresponding to (3) is

$$\begin{cases} S^{n+1} = \frac{S^n + h \alpha + h\omega R^n}{((1 + h(\beta I^n + \mu))}, \\ E^{n+1} = \frac{E^n + h\beta S^{n-m+1}(t - \tau)I^{n-m}(t - \tau)e^{-\mu\tau}}{1 + h(\varphi + \mu)}, \\ I^{n+1} = \frac{I^n + h\varphi E^n}{1 + h(\sigma + \delta + \mu)}, \\ R^{n+1} = \frac{R^n + h\sigma I^n}{1 + h(\mu + \omega)}. \end{cases} \tag{29}$$

### 4.4 Positivity of the NSFD Scheme

Since all state variables within the model represent proportions of a population, it follows that something like one of them should be positive, while the others should remain non-negative consistently. In this context, the theorem presented below provides valuable insight.

**Theorem:** Assume that  $S \geq 0$ ,  $E \geq 0$ ,  $I \geq 0$ , and  $R \geq 0$  are all positive at  $t = 0$ ; furthermore,  $\alpha \geq 0$ ,  $\delta \geq 0$ ,  $\mu \geq 0$ ,  $\omega \geq 0$ ,  $\sigma \geq 0$ ,  $\varphi \geq 0$ ,  $\tau \geq 0$ , and  $\beta \geq 0$  then  $S^{n+1} \geq 0$ ,  $E^{n+1} \geq 0$ ,  $I^{n+1} \geq 0$ , and  $R^{n+1} \geq 0$ .  $\forall n \in \mathbb{Z}^+ = \{0, 1, 2, 3, \dots\}$ .

**Proof:** Now for  $n = 0$ , system (29) becomes

$$\begin{cases} S^1 = \frac{S^0 + h \alpha + h\omega R^0}{((1 + h(\beta I^0 + \mu))} \geq 0, \\ E^1 = \frac{E^0 + h\beta S^0 I^0 e^{-\mu\tau}}{1 + h(\varphi + \mu)} \geq 0, \\ I^1 = \frac{I^0 + h\varphi E^0}{1 + h(\sigma + \delta + \mu)} \geq 0, \\ R^1 = \frac{R^0 + h\sigma I^0}{1 + h(\mu + \omega)} \geq 0. \end{cases} \tag{30}$$

Now for  $n = 1$ , system (29) becomes

$$\begin{cases} S^2 = \frac{S^1 + h\alpha + h\omega R^1}{(1 + h(\beta I^1 + \mu))} \geq 0, \\ E^2 = \frac{E^1 + h\beta S^1 I^1 e^{-\mu\tau}}{1 + h(\varphi + \mu)} \geq 0, \\ I^2 = \frac{I^1 + h\varphi E^1}{1 + h(\sigma + \delta + \mu)} \geq 0, \\ R^2 = \frac{R^1 + h\sigma I^1}{1 + h(\mu + \omega)} \geq 0. \end{cases} \quad (31)$$

The study assumes that the preceding set of equations guarantees that the values of  $S$ ,  $E$ ,  $I$  and  $R$  have the property of positivity for  $n = 2, 3, 4, \dots, n-1$ . In other words, for  $n = 2, 3, 4, \dots, n-1$ ,  $S^{n+1} \geq 0$ ,  $E^{n+1} \geq 0$ ,  $I^{n+1} \geq 0$  and  $R^{n+1} \geq 0$ . The positivity will now be investigated for a random positive integer  $n$ , and the system (29) becomes

$$\begin{cases} S^{n+1} = \frac{S^n + h\alpha + h\omega R^n}{(1 + h(\beta I^n + \mu))} \geq 0, \\ E^{n+1} = \frac{E^n + h\beta S^n I^n e^{-\mu\tau}}{1 + h(\varphi + \mu)} \geq 0, \\ I^{n+1} = \frac{I^n + h\varphi E^n}{1 + h(\sigma + \delta + \mu)} \geq 0, \\ R^{n+1} = \frac{R^n + h\sigma I^n}{1 + h(\mu + \omega)} \geq 0. \end{cases} \quad (32)$$

Obviously,  $S^{n+1} \geq 0$ ,  $E^{n+1} \geq 0$ ,  $I^{n+1} \geq 0$ , and  $R^{n+1} \geq 0$ , hence the proof.

#### 4.5 Boundedness of NSFD Scheme

Given that the model is about the human population, it is critical to ensure that at any given time  $t$ , the sum of populations in all compartments does not exceed the overall population. The following theorem addresses this condition effectively:

**Theorem:** Let  $S \geq 0$ ,  $E \geq 0$ ,  $I \geq 0$  and  $R \geq 0$  are finite, such that  $S + E + I + R \leq N$ ; furthermore,  $\alpha \geq 0$ ,  $\delta \geq 0$ ,  $\mu \geq 0$ ,  $\omega \geq 0$ ,  $\sigma \geq 0$ ,  $\varphi \geq 0$ ,  $\tau \geq 0$ , and  $\beta \geq 0$  then there is a constant such that  $S^{n+1} + E^{n+1} + I^{n+1} + R^{n+1} \leq N_n$  for all  $n \in \mathbb{Z}^+$ .

**Proof:** For boundedness of the proposed NSFD scheme from above, the following can be obtained:

$$\begin{aligned} & S^{n+1}(1 + h(\beta I^n + \mu)) + E^{n+1}(1 + h(\varphi + \mu)) + I^{n+1}(1 + h(\sigma + \delta + \mu)) + R^{n+1}(1 + h(\mu + \omega)) \\ &= S^n + h\alpha + h\omega R^n + E^n + h\beta S^n I^n e^{-\mu\tau} + I^n + h\varphi E^n + R^n + h\sigma I^n, \end{aligned} \quad (33)$$

$$\begin{aligned} & (S^{n+1} + I^{n+1} + E^{n+1} + R^{n+1})(1 + h\mu) + h\beta I^n + h(\varphi + \sigma + \delta + \omega) \\ &= (S^n + I^n + E^n + R^n) + h(\alpha + h\omega R^n) + h(\beta S^n I^n e^{-\mu\tau} + \delta I^n + \varphi E^n + \sigma I^n), \end{aligned} \quad (34)$$

$$(S^{n+1} + I^{n+1} + E^{n+1} + R^{n+1}) + C = \frac{(S^n + I^n + E^n + R^n) + h(\alpha + h\omega R^n) + h(\beta S^n I^n e^{-\mu\tau} + \delta I^n + \varphi E^n + \sigma I^n)}{(1 + h\mu)},$$

Now for  $n = 0$  system, the above equation becomes

$$(S^1 + I^1 + E^1 + R^1) + C = \frac{(S^0 + I^0 + E^0 + R^0) + h(\alpha + h\omega R^0) + h(\beta S^0 I^0 e^{-\mu\tau} + \delta I^0 + \varphi E^0 + \sigma I^0)}{(1 + h\mu)},$$

Since  $N_1 = S^0 + E^0 + I^0 + R^0$ , and  $S^1 + E^1 + I^1 + R^1 \leq N_1$ . Similarly, for  $n \in \mathbb{Z}^+$ , the above equation becomes

$$(S^{n+1} + I^{n+1} + E^{n+1} + R^{n+1}) + C = \frac{(S^n + I^n + E^n + R^n) + h(\alpha + h\omega R^n) + h(\beta S^n I^n e^{-\mu\tau} + \delta I^n + \varphi E^n + \sigma I^n)}{(1 + h\mu)}.$$

Consequently  $S^{n+1} \leq N_n, E^{n+1} \leq N_n, I^{n+1} \leq N_n$  and  $R^{n+1} \leq N_n$ , hence the proof.

#### 4.6 Convergence Analysis of NSF D Scheme

Let

$$\begin{cases} f^* = \frac{S + h\alpha + h\omega R}{(1 + h(\beta I + \mu))}, \\ g^* = \frac{E + h\beta S I e^{-\mu\tau}}{1 + h(\varphi + \mu)}, \\ q^* = \frac{I + h\varphi E}{1 + h(\sigma + \delta + \mu)}, \\ r^* = \frac{R + h\sigma I}{1 + h(\mu + \omega)}. \end{cases} \tag{35}$$

The Jacobian matrix of the system (35) at the DFE point is given below:

$$J^* = \begin{bmatrix} \frac{1}{(1 + h\mu)} & 0 & \frac{-h\beta\alpha}{\mu(1 + h\mu)} & \frac{h\omega}{1 + h\mu} \\ 0 & \frac{\mu + h\beta\alpha e^{-\mu\tau}}{\mu(1 + hk_1)} & \frac{1}{1 + hk_1} & 0 \\ 0 & \frac{h\varphi}{1 + hk_2} & \frac{1}{1 + hk_2} & 0 \\ 0 & 0 & \frac{h\sigma}{1 + hk_3} & \frac{1}{1 + hk_3} \end{bmatrix}.$$

For the above Jacobian matrix, it has eigenvalues  $\lambda_{d1} = 0.7385, \lambda_{d2} = 0.7279, \lambda_{d3} = 0.4003$  and  $\lambda_{d4} = 0.9902$ . Clearly,  $\lambda_{d1} < 1, \lambda_{d2} < 1, \lambda_{d3} < 1$  and  $\lambda_{d4} < 1$ . Hence, the proposed NSF D scheme is convergent.

#### 4.7 Consistency of NSF D Scheme

Beginning with the first equation in the system (29), then

$$S^{n+1} (1 + h(\beta I^n + \mu)) = S^n + h\alpha + h\omega R^n, \tag{36}$$

The Taylor's series expansion of the  $S^{n+1}$  is as follows:

$$S^{n+1} = \left( S^n + h \frac{dS}{dt} + \frac{h^2}{2!} \frac{d^2S}{dt^2} + \frac{h^3}{3!} \frac{d^3S}{dt^3} + \dots \right). \quad (37)$$

The following can be obtained from Eq. (36):

$$\left( S^n + h \frac{dS}{dt} + \frac{h^2}{2!} \frac{d^2S}{dt^2} + \frac{h^3}{3!} \frac{d^3S}{dt^3} + \dots \right) (1 + h(\beta I^n + \mu)) = S^n + h \alpha + h\omega R^n,$$

After some simplification and applying  $h \rightarrow 0$ , then

$$\begin{aligned} S^n(\beta I^n + \mu) + \frac{dS}{dt} &= \alpha + \omega R^n, \\ \frac{dS}{dt} &= \alpha - \beta S^n I^n + \omega R^n - \mu S^n, \\ \implies \frac{dS}{dt} &= \alpha - \beta S^n I^n + \omega R^n - \mu S^n. \end{aligned}$$

From the second equation of the NSFD scheme, it can have

$$E^{n+1}(1 + h(\varphi + \mu)) = E^n + h\beta S^n I^n e^{-\mu\tau}, \quad (38)$$

The Taylor's series expansion of the  $E^{n+1}$  is as follows:

$$E^{n+1} = \left( E^n + h \frac{dE}{dt} + \frac{h^2}{2!} \frac{d^2E}{dt^2} + \frac{h^3}{3!} \frac{d^3E}{dt^3} + \dots \right). \quad (39)$$

Substituting the value of  $E^{n+1}$  in (38), it can obtain

$$\left( E^n + h \frac{dE}{dt} + \frac{h^2}{2!} \frac{d^2E}{dt^2} + \frac{h^3}{3!} \frac{d^3E}{dt^3} + \dots \right) (1 + h(\varphi + \mu)) = E^n + h\beta S^n I^n e^{-\mu\tau},$$

Apply  $h \rightarrow 0$ , then

$$\begin{aligned} E^n(\varphi + \mu) + \frac{dE}{dt} &= \beta S^n I^n e^{-\mu\tau}, \\ \frac{dE}{dt} &= \beta S^n I^n e^{-\mu\tau} - E^n(\varphi + \mu), \\ \implies \frac{dE}{dt} &= \beta S^n I^n e^{-\mu\tau} - E^n(\varphi + \mu) \end{aligned}$$

From the third equation of the NSFD scheme, the following can be obtained:

$$I^{n+1}(1 + h(\sigma + \delta + \mu)) = I^n + h\varphi E^n, \quad (40)$$

The Taylor's series expansion of the  $I^{n+1}$  is as follows:

$$I^{n+1} = \left( I^n + h \frac{dI}{dt} + \frac{h^2}{2!} \frac{d^2I}{dt^2} + \frac{h^3}{3!} \frac{d^3I}{dt^3} + \dots \right), \quad (41)$$

$$\left( I^n + h \frac{dI}{dt} + \frac{h^2}{2!} \frac{d^2I}{dt^2} + \frac{h^3}{3!} \frac{d^3I}{dt^3} + \dots \right) (1 + h(\sigma + \delta + \mu)) = I^n + h\varphi E^n,$$

By applying  $h \rightarrow 0$ , the following can be obtained:

$$I^n (\sigma + \delta + \mu) + \frac{dI}{dt} = \varphi E^n,$$

$$\frac{dI}{dt} = \varphi E^n - I^n (\sigma + \delta + \mu).$$

$$\implies \frac{dI}{dt} = \varphi E^n - I^n (\sigma + \delta + \mu).$$

From the fourth equation of the NSFD scheme, it can have

$$R^{n+1} (1 + h(\mu + \omega)) = R^n + h\sigma I^n, \tag{42}$$

The Taylor's series expansion of the  $R^{n+1}$  is as follows:

$$R^{n+1} = \left( R^n + h \frac{dR}{dt} + \frac{h^2}{2!} \frac{d^2R}{dt^2} + \frac{h^3}{3!} \frac{d^3R}{dt^3} + \dots \right), \tag{43}$$

Similarly,

$$\frac{dR}{dt} = \delta I^n - R^n (\mu + \omega)$$

by substituting (42) in (43) and simplifying it. Hence, the proposed NSFD scheme with the delay effect is consistent with the first order.

#### 4.8 Global Stability

By demonstrating global stability, the study provides strong theoretical support for using time-delayed models to understand and manage typhoid fever outbreaks.

##### Case 1: Trivial Case

Consider a candidate Lyapunov function as follows:

$$L_1(t) = S(t) + E(t) + I(t) + R(t), \tag{44}$$

$$L_1(t) = \frac{dS}{dt} + \frac{dE}{dt} + \frac{dI}{dt} + \frac{dR}{dt}, \tag{45}$$

$$L_1(t) = \alpha - \mu(S + E + I + R) - \delta I, \tag{46}$$

$$L_1(t) = \alpha - \mu N - \delta I, \tag{47}$$

$$L_1(t) \leq 0.$$

##### Case 2: Disease-Free Equilibrium

Consider Volterra type Lyapunov function it can have

$$\frac{d\Delta}{dt} = \frac{d}{dt} (S - S^* \ln S) + \frac{dE}{dt} + \frac{dI}{dt} + \frac{dR}{dt}, \tag{48}$$

$$\frac{d\Delta}{dt} \leq \left(1 - \frac{S^*}{S}\right) \frac{dS}{dt} + \frac{dE}{dt} + \frac{dI}{dt} + \frac{dR}{dt},$$

$$\frac{d\Delta}{dt} \leq \left(-\frac{S^*}{S}\right) \frac{dS}{dt} + \frac{dE}{dt} + \frac{dI}{dt} + \frac{dR}{dt},$$

$$\frac{d\Delta}{dt} \leq \left(-\frac{S^*}{S}\right) \frac{dS}{dt} + 0,$$

$$\frac{d\Delta}{dt} \leq 0.$$

Case 3: Endemic Equilibrium

$$\Delta(S, E, I, R) = \mathcal{K}_1(S - S^* \ln S) + \mathcal{K}_2(E - E^* \ln E) + \mathcal{K}_3(I - I^* \ln I) + \mathcal{K}_4(R - R^* \ln R), \quad (49)$$

$$\begin{aligned} \frac{d}{dt} \Delta(S, E, I, R) = & \mathcal{K}_1 \frac{d}{dt} (S - S^* \ln S) + \mathcal{K}_2 \frac{d}{dt} (E - E^* \ln E) \\ & + \mathcal{K}_3 \frac{d}{dt} (I - I^* \ln I) + \mathcal{K}_4 \frac{d}{dt} (R - R^* \ln R), \end{aligned} \quad (50)$$

$$\frac{d\Delta}{dt} \leq \mathcal{K}_1 \left(1 - \frac{S^*}{S}\right) \frac{dS}{dt} + \mathcal{K}_2 \left(1 - \frac{E^*}{E}\right) \frac{dE}{dt} + \mathcal{K}_3 \left(1 - \frac{I^*}{I}\right) \frac{dI}{dt} + \mathcal{K}_4 \left(1 - \frac{R^*}{R}\right) \frac{dR}{dt},$$

$$\frac{d\Delta}{dt} \leq \mathcal{K}_1 \left(\frac{S - S^*}{S}\right) \frac{dS}{dt} + \mathcal{K}_2 \left(\frac{E - E^*}{E}\right) \frac{dE}{dt} + \mathcal{K}_3 \left(\frac{I - I^*}{I}\right) \frac{dI}{dt} + \mathcal{K}_4 \left(\frac{R - R^*}{R}\right) \frac{dR}{dt},$$

$$\frac{d\Delta}{dt} \leq \mathcal{K}_1 (S - S^*) \left(\frac{\alpha}{S} + \frac{\omega R}{S} - (\beta I + \mu)\right) + \mathcal{K}_2 (E - E^*) \left(\frac{\beta S I e^{-\mu\tau}}{E} - (\varphi + \mu)\right) +$$

$$\mathcal{K}_3 (I - I^*) \left(\frac{\varphi E}{I} - (\sigma + \delta + \mu)\right) + \mathcal{K}_4 (R - R^*) \left(\frac{\sigma I}{R} - (\omega + \mu)\right).$$

From the first equations of system (3)

$$\alpha - \beta S^* I + \omega R - \mu S^* = 0,$$

$$\beta I + \mu = \frac{\alpha}{S^*} + \frac{\omega R}{S^*}.$$

From the second equation of system (3)

$$\beta S I e^{-\mu\tau} - \varphi E^* - \mu E^* = 0,$$

$$\varphi + \mu = \frac{\beta S I e^{-\mu\tau}}{E^*}.$$

From the third equation of system (3)

$$\varphi E - \sigma I^* - \delta I^* - \mu I^* = 0,$$

$$\sigma + \delta + \mu = \frac{\varphi E}{I^*}.$$

From the fourth equation of system (3)

$$\sigma I - \omega R^* - \mu R^* = 0,$$

$$\omega + \mu = \frac{\sigma I}{R^*}.$$

Now, it can have

$$\begin{aligned} \frac{d\Delta}{dt} \leq & \mathcal{K}_1 (S - S^*) \left( \frac{\alpha}{S} + \frac{\omega R}{S} - \frac{\alpha}{S^*} + \frac{\omega R}{S^*} \right) + \mathcal{K}_2 (E - E^*) \left( \frac{\beta S I e^{-\mu\tau}}{E} - \frac{\beta S I e^{-\mu\tau}}{E^*} \right) \\ & + \mathcal{K}_3 (I - I^*) \left( \frac{\varphi E}{I} - \frac{\varphi E}{I^*} \right) + \mathcal{K}_4 (R - R^*) \left( \frac{\sigma I}{R} - \frac{\sigma I}{R^*} \right), \end{aligned}$$

$$\begin{aligned} \frac{d\Delta}{dt} \leq & - \mathcal{K}_1 (S - S^*)^2 \left( \frac{\alpha + \omega R}{SS^*} \right) - \mathcal{K}_2 (E - E^*)^2 \left( \frac{\beta S I e^{-\mu\tau}}{EE^*} \right) - \mathcal{K}_3 (I - I^*)^2 \left( \frac{\varphi E}{II^*} \right) \\ & - \mathcal{K}_4 (R - R^*)^2 \left( \frac{\sigma I}{RR^*} \right). \end{aligned}$$

Hence, set  $\mathcal{K}_1 = \mathcal{K}_2 = \mathcal{K}_3 = \mathcal{K}_4 = 1$ .

## 5 Numerical Simulations

Table 1 lists the parameters employed in numerical simulations, while Table 2 details the initial conditions. The figures illustrate the dynamics of a delayed SEIR model.

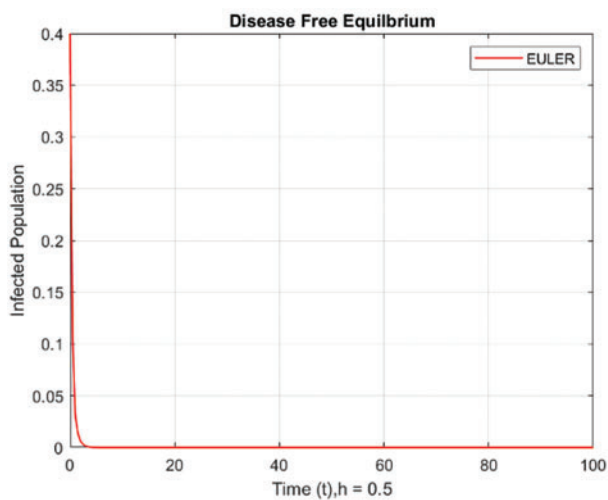
In Fig. 2, the forward Euler technique displays favorable behavior, converging at the DFE point with a small step size  $h = 0.5$ . However, as the step size increases in Fig. 3, the forward Euler method starts generating non-physical oscillations, which are irrelevant in disease dynamics due to the impossibility of negative counts. Fig. 4 indicates that the RK-4 technique exhibits commendable behavior, converging at the DFE point with a small step size  $h = 0.5$ . Nevertheless, in Fig. 5, as the step size increases, the RK-4 technique introduces negative aspects that are incongruent with disease dynamics since negative counts are implausible. Even though the approach to equilibrium states is gradual and has small step sizes, even a slight increase causes a deviation from this pattern. The test of RK-4 in keeping up with energy with bigger step sizes highlights its constraints in evaluating long-haul viral plague elements. In contrast, the NSFD scheme is insensitive to changes in step size because it remains positive, stable, and convergent regardless of step size. This particular capability is separated from customary methodologies. Fig. 6 exhibits the positive way of behaving and the combination of the NSFD technique at the DFE point with a small step size  $h = 0.5$ . In addition, Fig. 7 demonstrates the superiority of the NSFD method by confirming its effectiveness in modeling disease dynamics and demonstrating constant convergence across step size variations.

**Table 1:** Values of parameters

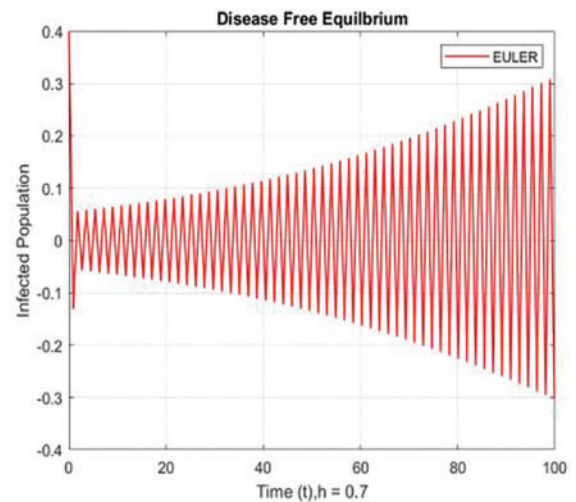
Parameters	Values
$\alpha$	5
$\beta$	0.5 (DFE) 4.5 (EE)
$\delta$	0.05
$\mu$	0.9
$\omega$	0.05
$\sigma$	0.9
$\varphi$	0.5
$\tau$	$\geq 0$

**Table 2:** Values of initial conditions

Symbols	Values
$S(0)$	0.2
$E(0)$	0.3
$I(0)$	0.4
$R(0)$	0.5



(a)



(b)

**Figure 2:** Infected populations at various step sizes employing the Euler approach. (a)  $h = 0.5$ , (b)  $h = 0.7$



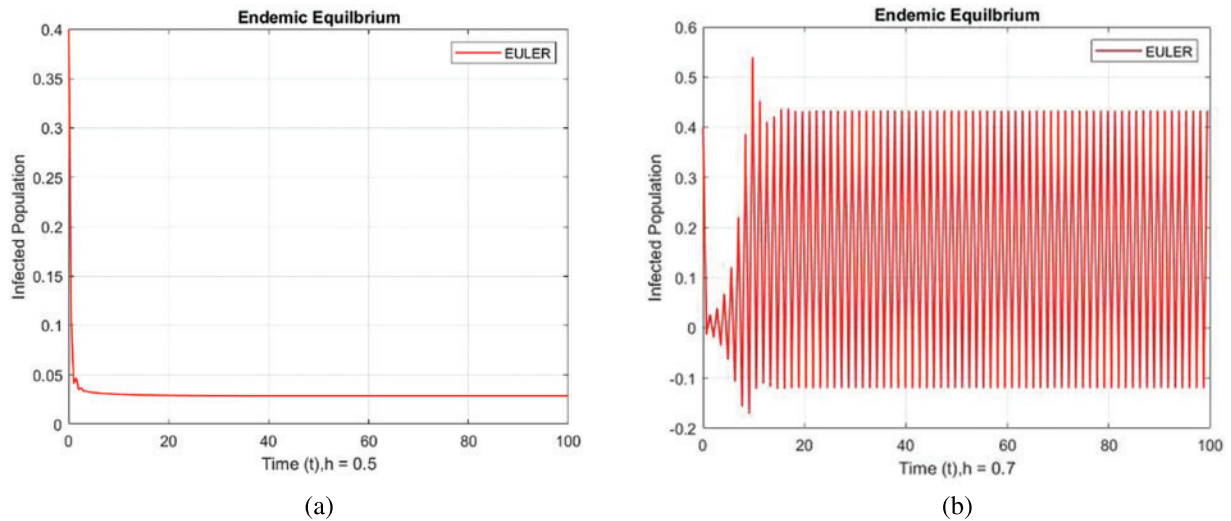


**Figure 3:** Infected populations at various step sizes employing the Euler approach. (a)  $h = 0.5$ , (b)  $h = 0.7$

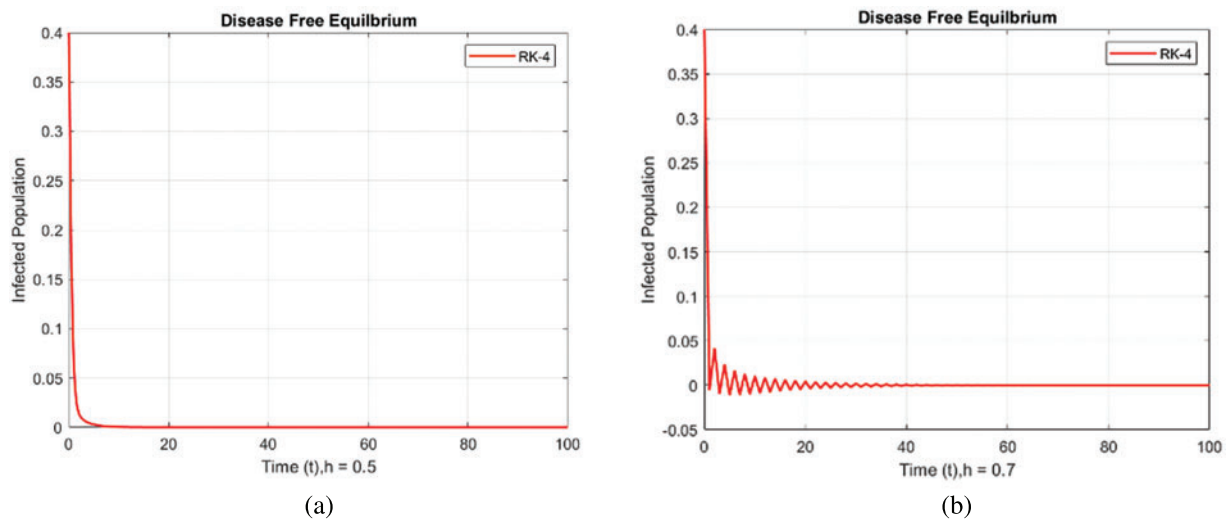


**Figure 4:** Infected populations at various step sizes employing the RK-4 approach. (a)  $h = 0.5$ , (b)  $h = 0.7$

Figs. 8 and 9 compare the infected population of a model with and without a time delay factor. The Euler Method demonstrates that introducing a delay can control the endemic status. On the other hand, Figs. 10 and 11 show the behavior of the infected population using the RK-4 approach, resulting in a delay in people getting infected after adding a delay factor in the exposed compartment. In addition, Figs. 12 and 13 indicate that the NSFD scheme is more convergent in a delayed model than without a delay. Fig. 14 outlines charts of infected populations for different values of  $\tau$ . A reliable perception arose through these mathematical tests: The exposed population decreases as the delay factor increases. Finally, Fig. 15 shows a comparison of  $R_{d_0}$  and demonstrates that an increase in  $\tau$  can transform an endemic state into a disease-free one. Fig. 16 clearly illustrates that the time

delay factor  $\tau$  is more beneficial in controlling the disease spread rate. This situation reflects genuine circumstances where a worldly postponement in transmitting any infectious infection can support its remediation or disposal, possibly impacted by factors like antivirus programming, programming refreshes, or the reception of deterrent measures. In synopsis, all approaches combine to a similar balance position at small step sizes. Euler and RK-4 methods, on the other hand, fail to converge as step sizes increase, exhibiting oscillations and negatives. In contrast, the NSFD method maintains convergence even at significantly larger step sizes, demonstrating its dependability in accurately describing disease dynamics.

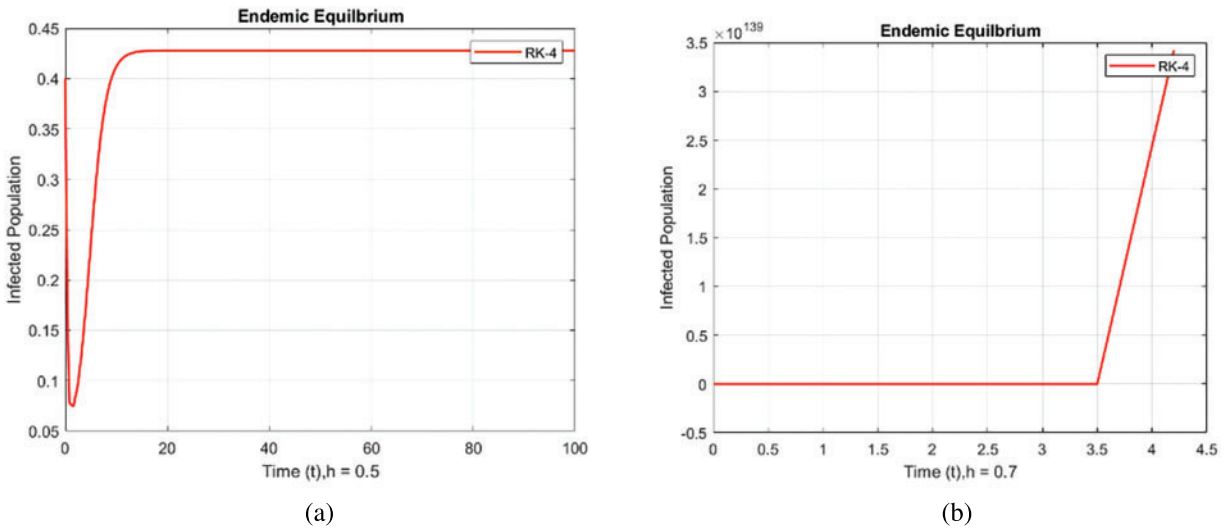


**Figure 5:** Infected populations at various step sizes employing the RK-4 approach. (a)  $h = 0.5$ , (b)  $h = 0.7$

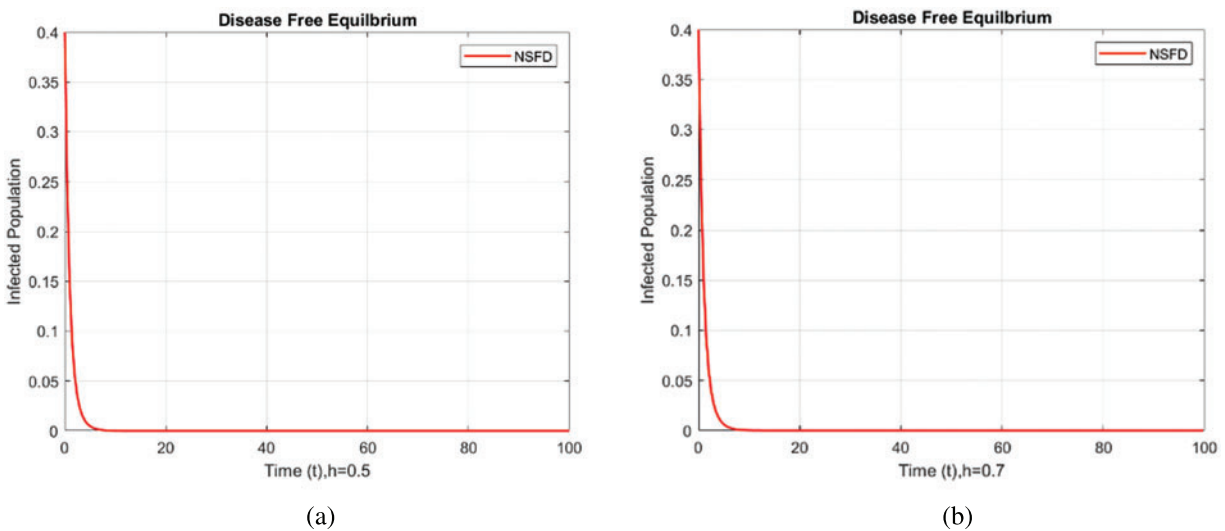


**Figure 6:** Infected populations at various step sizes employing the NSFD approach. (a)  $h = 0.5$ , (b)  $h = 0.7$

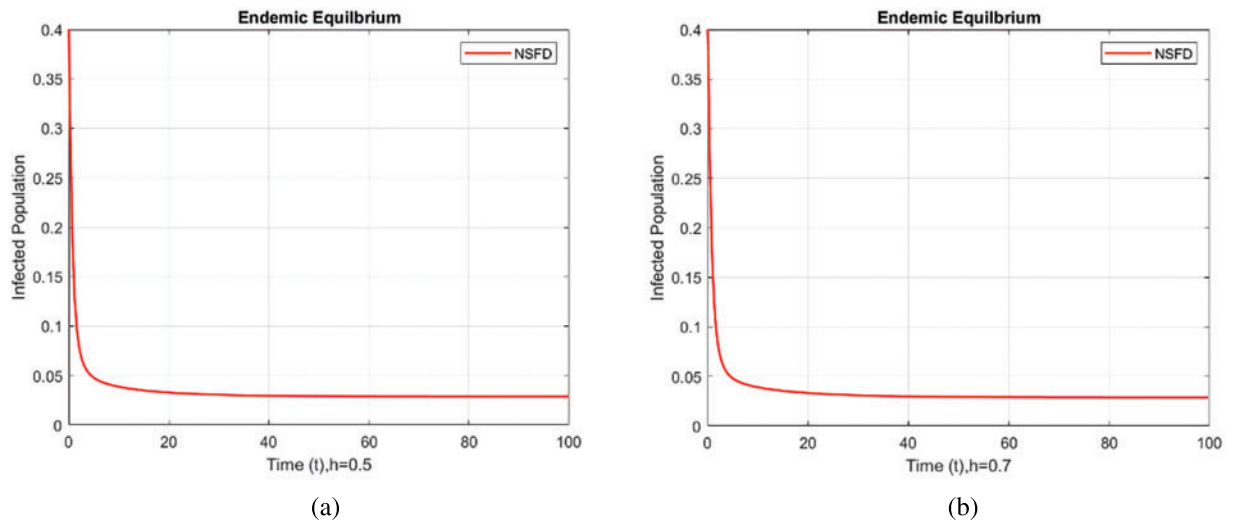


**Figure 7:** Infected populations at various step sizes employing the NSFD approach. (a)  $h = 0.5$ , (b)  $h = 0.7$

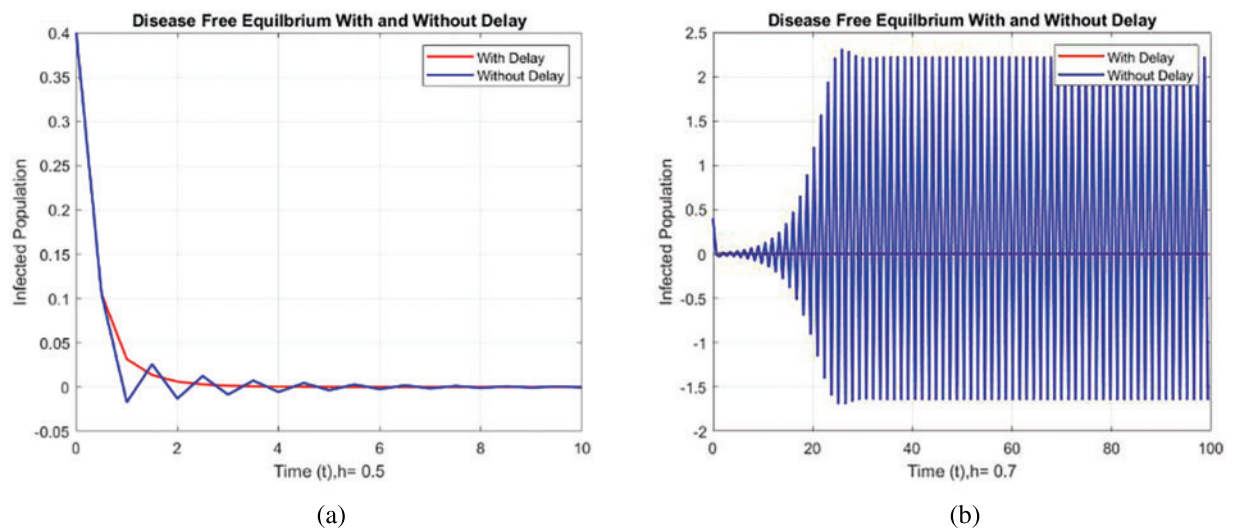


**Figure 8:** Comparison of the infected population at various step sizes employing the Euler approach. (a)  $h = 0.5$ , (b)  $h = 0.7$

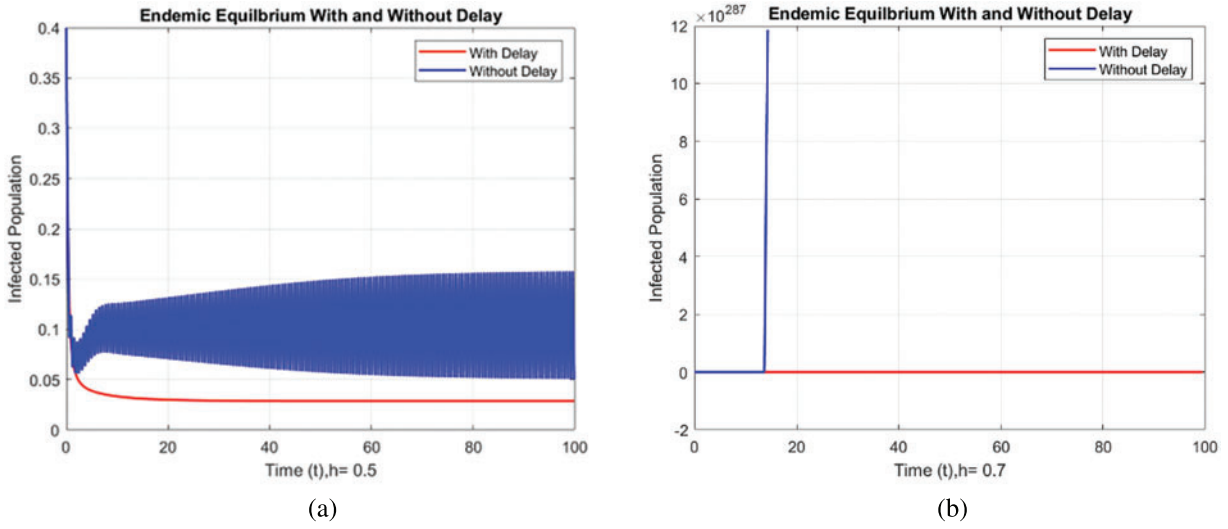


**Figure 9:** Comparison of the infected population at various step sizes employing the Euler approach. (a)  $h = 0.5$ , (b)  $h = 0.7$

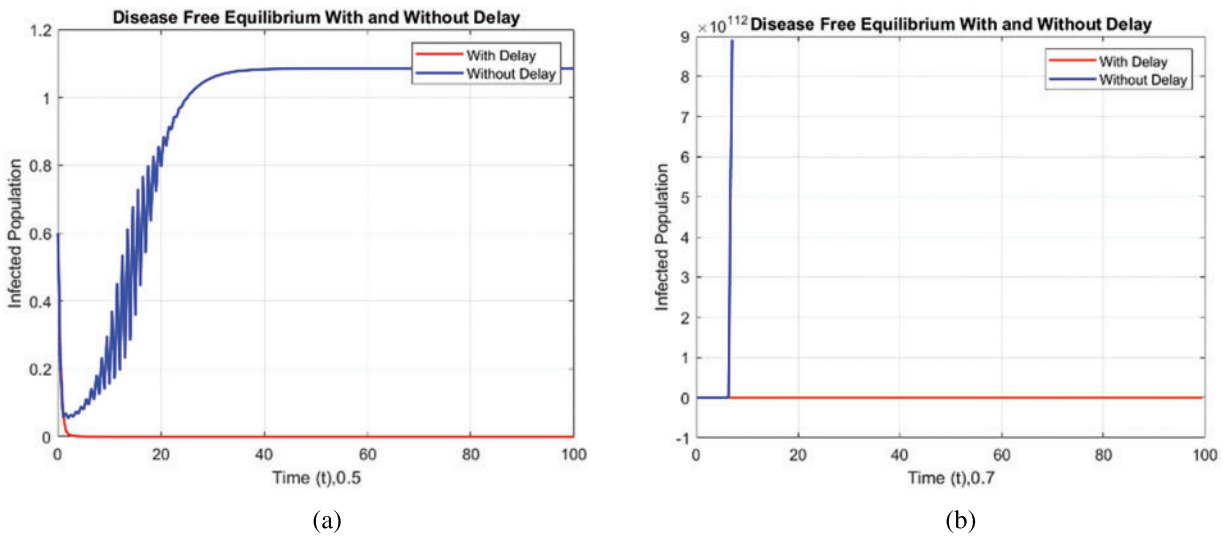
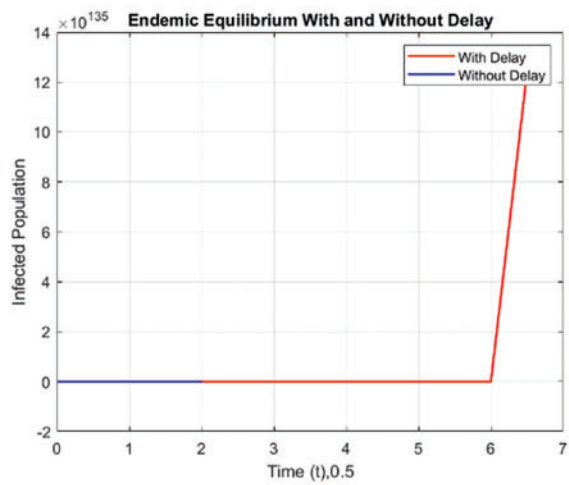
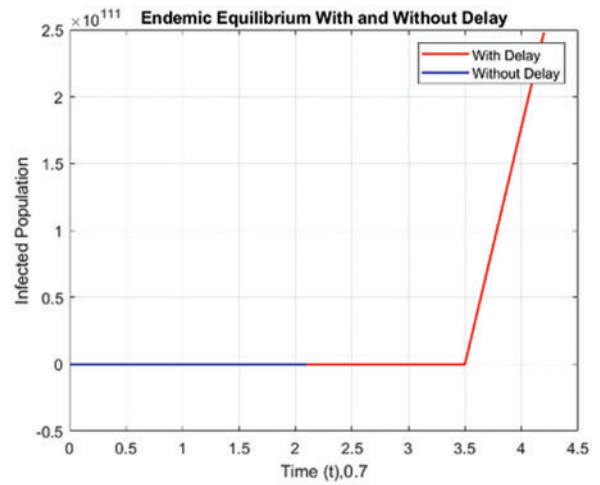


**Figure 10:** Comparison of the infected population at various step sizes employing the RK-4 approach. (a)  $h = 0.5$ , (b)  $h = 0.7$

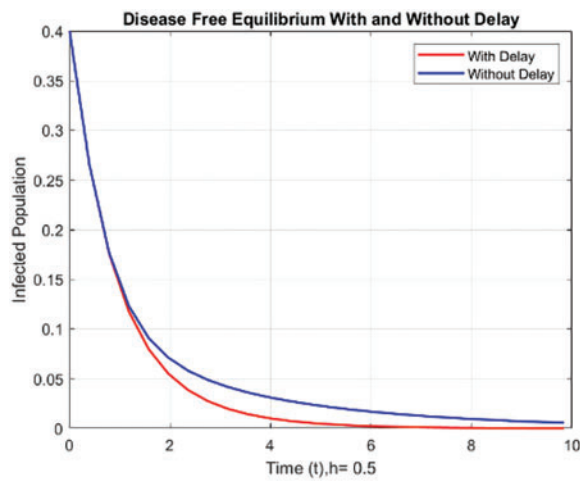


(a)

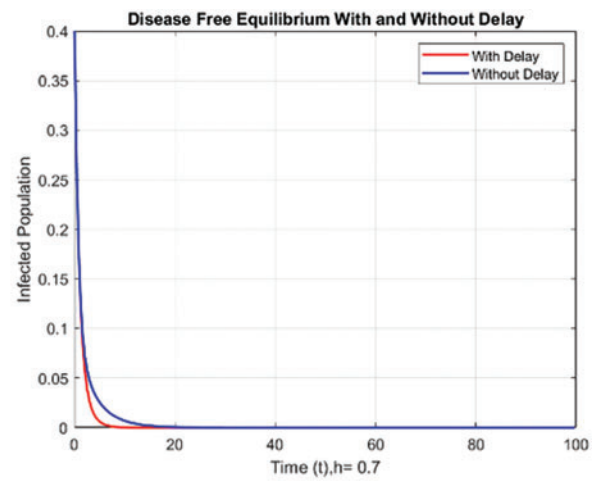


(b)

**Figure 11:** Comparison of the infected population at various step sizes employing the RK-4 approach. (a)  $h = 0.5$ , (b)  $h = 0.7$



(a)



(b)

**Figure 12:** Comparison of Infected population at various step sizes employing NSFD approach. (a)  $h = 0.5$ , (b)  $h = 0.7$

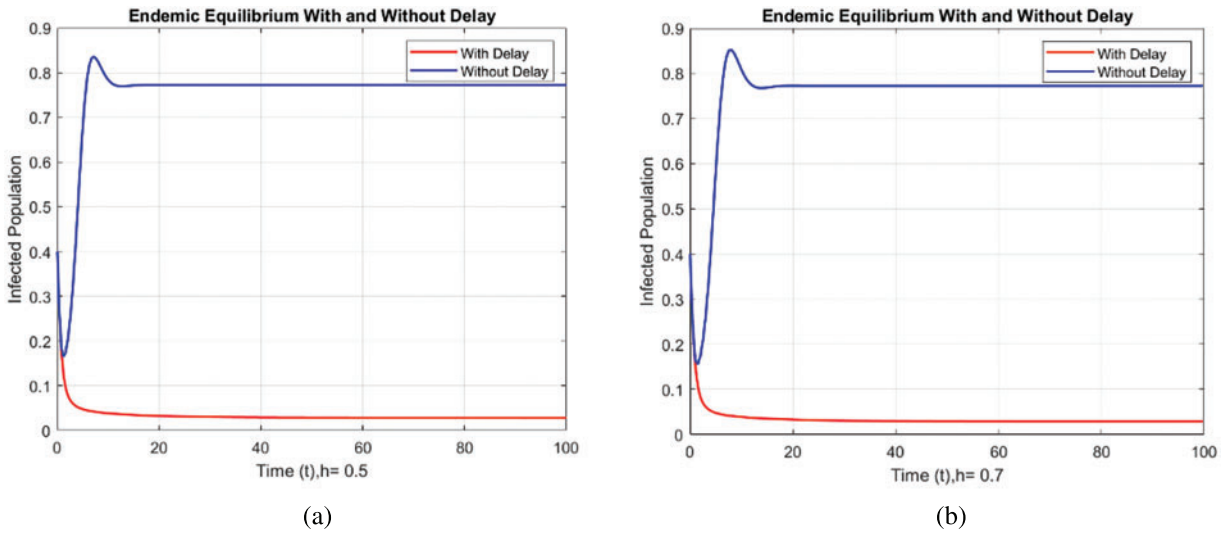


**Figure 13:** Comparison of the infected population at various step sizes employing NSFD approach. (a)  $h = 0.5$ , (b)  $h = 0.7$

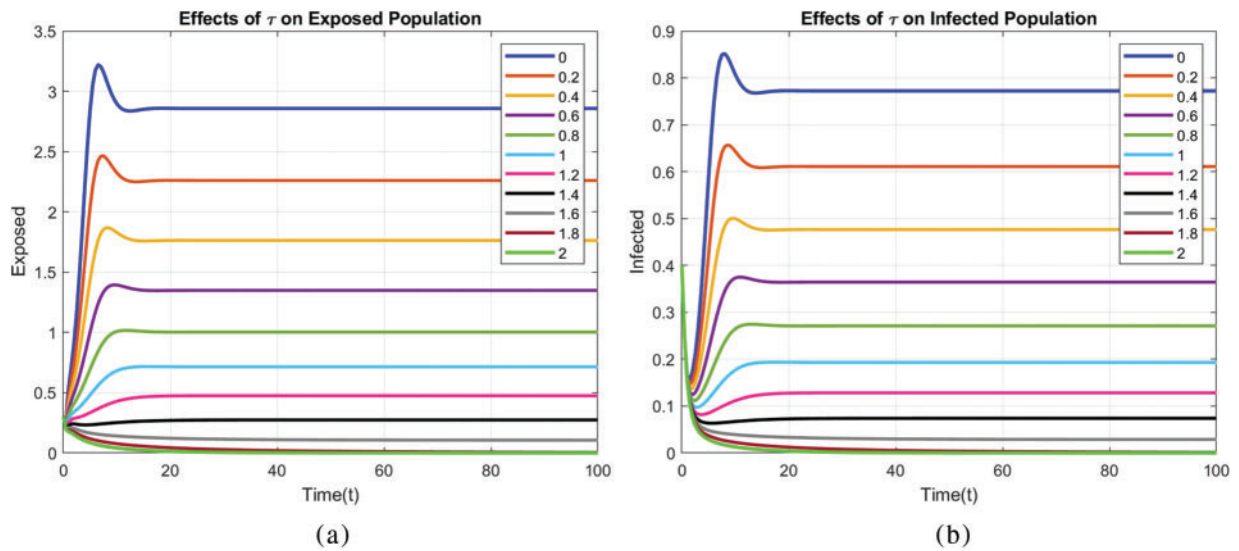


**Figure 14:** Effect of different values of  $\tau$  on population dynamics. (a) Effect on exposed population, (b) Effect on infected population

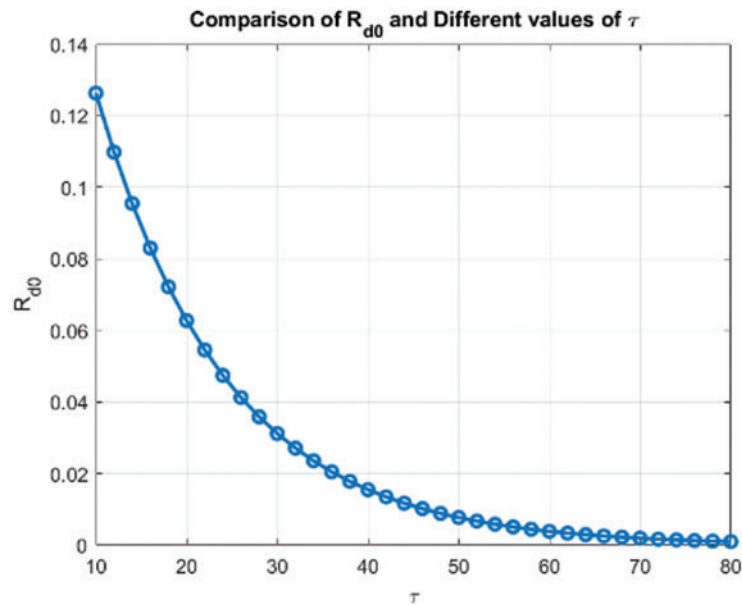


Figure 15: Comparison of  $R_{d0}$  and  $\tau$

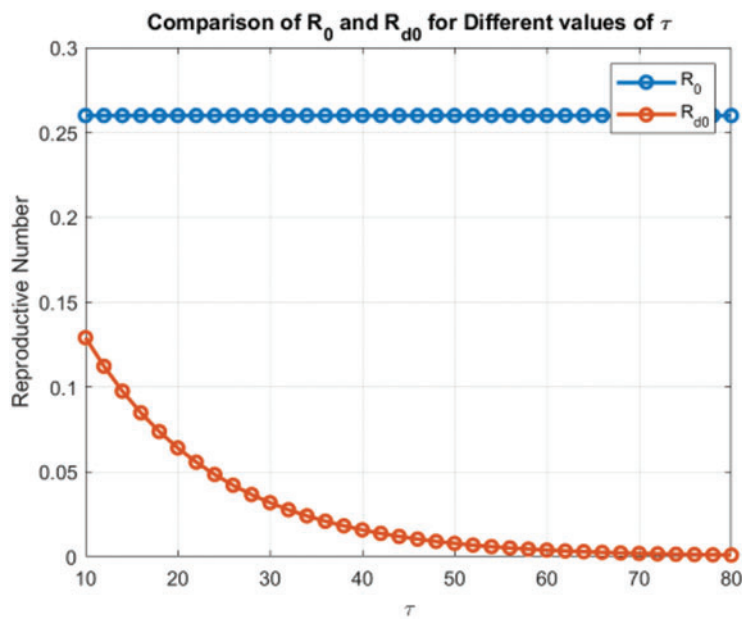


Figure 16: Comparison of  $R_{d0}$  and  $R_0$  for different values of  $\tau$

### 6 Parameter Estimation Analysis

A helpful way to validate the Typhoid delayed epidemic model is by fitting the model parameters to data obtained on the actual typhoid epidemics. All the data for Typhoid fever is collected and compiled from the Integrated Disease Surveillance & Response (IDSR) Report, Center of Disease Control, National Institute of Health, Islamabad. The data consists of the cases reported all over the

country for 2023 [42]. It enhances the model, hence a better appreciation of the disease pattern and a better prediction of the future status of the disease. The least squares method of curve fitting is employed to estimate the model's parameters. Now, it is possible to fit the model's parameters using the least squares approach using actual data regarding the newly infected typhoid cases in 2023, as indicated in Table 3. Among them, this study selected two parameters, incidence rate  $\varphi$ , and time delay  $\tau$ , and the remaining parameters provide better estimation based on the actual cases of typhoid fever in Pakistan. It was evident from the fitted model of the number of infected cases per month that the model was accurate in the sense that it predicted the number of infected cases each month. In Fig. 17, the red-filled circles represent the observed values explained in the previous section, while the continuous blue line shows the model's nonlinear least square curve fitting. This graph appears to indicate that the model in question works quite well in terms of how it addresses the numerical progression of the epidemics of typhoid fever in reality. When it was pointed out that the least squares method was used and the data was real, this ensures that the Typhoid delayed epidemic model indeed simulates the epidemic. In addition, the model can offer information regarding what can prevent the emergence of similar diseases in society in the future.

**Table 3:** Number of Typhoid fever surveillance reports in Pakistan in 2023

Months	Infected typhoid cases
January	3598
February	4669
March	6251
April	5446
May	12,166
June	17,527
July	27,176
August	42,321
September	29,414
October	23,257
November	29,200
December	23,383



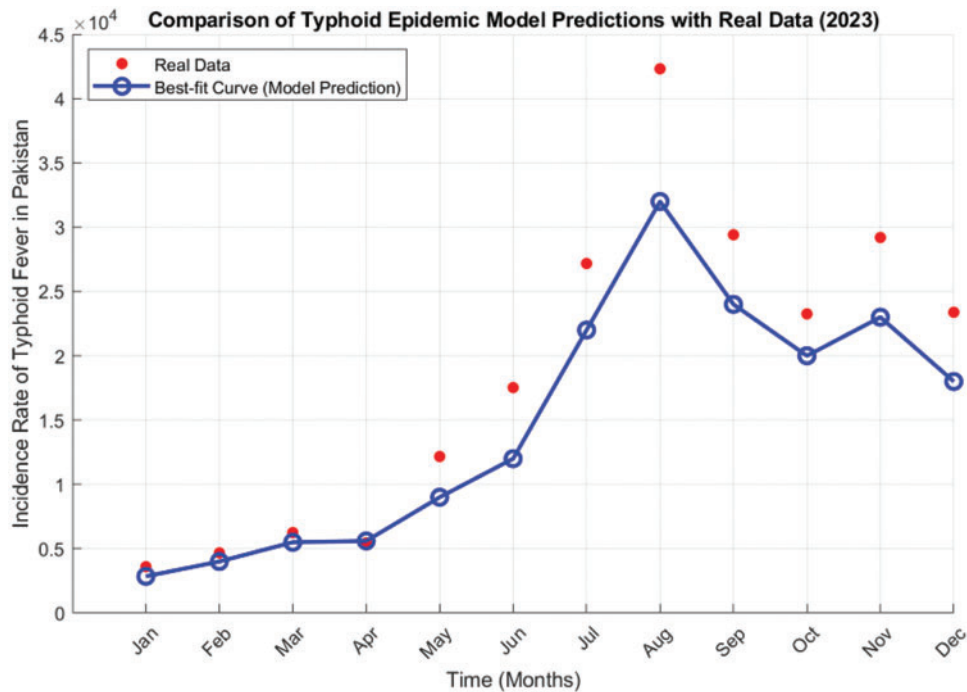


**Figure 17:** The monthly Typhoid fever cases time series in Pakistan for 2023 and the proposed model's best-fitted curve

## 7 Conclusion

The transmission of typhoid fever caused by *Salmonella typhi* is examined using a mathematical model that emphasizes the importance of delay in its effectiveness. Time delays can influence the nature of patterns and slow the emergence of patterns in the density of the infected population. The analyzed model is further expanded with equilibrium analysis, reproduction number calculation, and stability analysis. Three numerical techniques, forward Euler, RK-4, and NSFD, are employed to solve the proposed model. Some essential characteristics such as convergence, positivity, boundedness, and consistency are studied, and the developed scheme preserves all these essential features. The calculated results demonstrated the usefulness of the NSFD method in accurately capturing and preserving the essential characteristics of the continuous delayed model. It demonstrated that the proposed NSFD scheme maintains the integrity of the continuous delayed model's characteristics, positivity, boundedness, and asymptotic stability over all finite step sizes. As a result, it produces dependable approximations, whereas several traditional techniques fail to maintain the critical mathematical properties of the continuous model. As a result, these strategies create solutions that are not just unstable but also negative. Finally, numerical simulations were run to validate the results of the analytical research. This study intends to explore the development of higher-order NSFD schemes tailored for typhoid transmission models. Future directions could include stochastic, fractional, and fuzzy extensions, among other possibilities.

**Limitation of study:** In the present work, the previous mathematical model of the transmission of Typhoid fever is vindicated using time delay and the NSFD scheme. Some of the limitations include the following: This is a model that is built on some assumptions, and therefore, when obtaining such

data in real life, it is essential to check the credibility of the mentioned benchmarks. Still, it is as accurate as the epidemiological data with which the model was supplied, which might be limited or of uneven quality. The utilization of the NSFD scheme can be complex, especially in assigning it, and perhaps more complicated for those with little quantitative proficiency or in places with few resources since the modulated method entails some calculation. NSFD is superior to makeshift solutions, yet there is a specific aspect to consider when choosing a step size. Also, the model does not incorporate geographical factors and other aspects of the environment, which may be disadvantageous in a specific scenario. In order to address these limitations in subsequent studies, it is essential to continuously improve and validate the model to further enhance its usefulness in finding the right strategy for eradicating this health complication.

**Acknowledgement:** The authors Thabet Abdeljawad and Aiman Mukheimer would like to thank Prince Sultan University for paying the APC and for the support through TAS research lab.

**Funding Statement:** This work is supported by Prince Sultan University through TAS research lab.

**Author Contributions:** Conceptualization, methodology, software, and draft manuscript preparation: Muhammad Tashfeen and Fazal Dayan, Formal analysis, methodology, software, validation, and supervision: Muhammad Aziz ur Rehman, Thabet Abdeljawad and Aiman Mukheimer. All authors reviewed the results and approved the final version of the manuscript.

**Availability of Data and Materials:** The datasets used and/or analyzed during the current study are available from the corresponding author upon reasonable request.

**Ethics Approval:** Not applicable.

**Conflicts of Interest:** The authors declare that they have no conflicts of interest to report regarding the present study.

## References

1. Masasila NH, Ngeleja RC. Mathematical analysis of the role of information on the dynamics of typhoid fever; 2023. Available from: <https://arxiv.org/abs/2310.09825>. [Assessed 2024].
2. Ivanoff B, Levine MM, Lambert P. Vaccination against typhoid fever: present status. *Bull World Health Organ.* 1994;72(6):957.
3. Nsutebu EF, Martins P, Adiogo D. Prevalence of typhoid fever in febrile patients with symptoms clinically compatible with typhoid fever in Cameroon. *Trop Med Int Health.* 2003;8(6):575–8. doi:10.1046/j.1365-3156.2003.01012.x.
4. Shaikh AS, Nisar KS. Transmission dynamics of fractional-order typhoid fever model using Caputo-Fabrizio operator. *Chaos Solit Fractals.* 2019;128:355–65. doi:10.1016/j.chaos.2019.08.012.
5. Mushayabasa S. Modeling the impact of optimal screening on typhoid dynamics. *Int J Dyn Control.* 2016;4:330–8. doi:10.1007/s40435-014-0123-4.
6. Adegbola EY. Mathematical modeling of the transmission dynamics of typhoid fever and its control (Ph.D. Thesis). Federal University of Technology: Minna, Nigeria; 2023.
7. Suhuyini AK, Seidu B. A mathematical model on the transmission dynamics of typhoid fever with treatment and booster vaccination. *Front Appl Math Stat.* 2023;9:1151270. doi:10.3389/fams.2023.1151270.
8. Mushayabasa S, Bhunu CP, Ngarakana-Gwasira ET. Mathematical analysis of a typhoid model with carriers, direct and indirect disease transmission. *Int J Math Sci Eng Appl.* 2013;7(1):79–90.

9. Antillón M, Warren JL, Crawford FW, Weinberger DM, Kürüm E, Pak GD, et al. The burden of typhoid fever in low-and middle-income countries: a meta-regression approach. *PLoS Negl Trop Dis*. 2017;11(2):e0005376.
10. Punchihewage-Don AJ, Hawkins J, Adnan AM, Hashem F, Parveen S. The outbreaks and prevalence of antimicrobial resistant Salmonella in poultry in the United States: an overview. *Heliyon*. 2022;8(11):e11613.
11. Mushayabasa S. A simple epidemiological model for Typhoid with saturated incidence rate and treatment effect. *Int J Math Comput Sci*. 2013;6(6):688–95.
12. Nyerere N, Mpeshe SC, Edward S. Modeling the impact of screening and treatment on the dynamics of typhoid fever. *World J Model Simul*. 2018;14(4):298–306.
13. Karunditu JW, Kimathi G, Osman S. Mathematical modeling of typhoid fever disease incorporating unprotected humans in the spread dynamics. *J Adv Math Comput Sci*. 2019;32(3):1–11. doi:10.9734/jamcs/2019/v32i330144.
14. Mutua JM, Wang FB, Vaidya NK. Modeling malaria and typhoid fever co-infection dynamics. *Math Biosci*. 2015;264:128–44. doi:10.1016/j.mbs.2015.03.014.
15. Tilahun GT, Makinde OD, Malonza D. Co-dynamics of pneumonia and typhoid fever diseases with cost-effective optimal control analysis. *Appl Math Comput*. 2018;316:438–59. doi:10.1016/j.amc.2017.07.063.
16. Mushanyu J, Nyabadza F, Muchatibaya G, Mafuta P, Nhawu G. Assessing the potential impact of limited public health resources on the spread and control of Typhoid. *J Math Biol*. 2018;77:647–70. doi:10.1007/s00285-018-1219-9.
17. Alharbi MH, Alalhareth FK, Ibrahim MA. Analyzing the dynamics of a periodic typhoid fever transmission model with imperfect vaccination. *Mathematics*. 2023;11(15):3298. doi:10.3390/math11153298.
18. Edward S. A deterministic mathematical model for direct and indirect transmission dynamics of typhoid fever. *Open Access Libr J*. 2017;4(5):1–16.
19. Musa SS, Zhao S, Hussaini N, Usaini S, He D. Dynamics analysis of typhoid fever with public health education programs and final epidemic size relation. *Results Appl Math*. 2021;10:100153.
20. Peter OJ, Ibrahim MO, Edogbanya HO, Oguntolu FA, Oshinubi K, Ibrahim AA, et al. Direct and indirect transmission of typhoid fever model with optimal control. *Results Phys*. 2021;27:104463.
21. Edward S, Nyerere N. Modelling typhoid fever with education, vaccination and treatment. *Eng Math*. 2016;1(1):44–52.
22. Nwokoye CH, Umeh II. The SEIQR-V model: on a more accurate analytical characterization of malicious threat defense. *Int J Inf Technol Comput Sci*. 2017;9(12):28–37.
23. Wang C, Chai S. Hopf bifurcation of an SEIRS epidemic model with delays and vertical transmission in the network. *Adv Differ Equ*. 2016;2016(1):1–19. doi:10.1186/s13662-016-0793-7.
24. Bailey NT. *The mathematical theory of infectious diseases and its applications*. London: Charles Griffin & Company Ltd.; 1975.
25. Suleman M, Riaz S. Unconditionally stable numerical scheme to study the dynamics of hepatitis B disease. *Punjab Univ J Math*. 2017;49(3):99–118.
26. World Health Organization. Typhoid vaccines: WHO position paper, March 2018–recommendations. *Vaccine*. 2019;37(2):214–6.
27. Sulaiman W. Typhoid and malaria co-infection-an interesting finding in the investigation of a tropical fever. *Malays J Med Sci*. 2006;13(2):64.
28. Saade M, Ghosh S, Banerjee M, Volpert V. Delay epidemic models determined by latency, infection, and immunity duration. *Math Biosci*. 2024;370:109155. doi:10.1016/j.mbs.2024.109155.
29. Jiang J, Zhou T. The influence of time delay on epidemic spreading under limited resources. *Physica A*. 2018;508:414–23. doi:10.1016/j.physa.2018.05.114.

30. Guglielmi N, Iacomini E, Viguierie A. Delay differential equations for the spatially resolved simulation of epidemics with specific application to COVID-19. *Math Methods Appl Sci.* 2022;45(8):4752–71. doi:10.1002/mma.8068.
31. Yau MA. Analysis of spatial dynamics and time delays in epidemic models (Ph.D. Thesis). University of Sussex: Brighton, UK; 2014.
32. Das K, Chinnathambi R, Srinivas MN, Rihan FA. An analysis of time-delay epidemic model for TB, HIV, and AIDS co-infections. *Results Control Optim.* 2023;12:100263. doi:10.1016/j.rico.2023.100263.
33. Goel K, Nilam. A mathematical and numerical study of a SIR epidemic model with time delay, nonlinear incidence and treatment rates. *Theory Biosci.* 2019;138(2):203–13. doi:10.1007/s12064-019-00275-5.
34. Ghosh S, Volpert V, Banerjee M. An epidemic model with time delay determined by the disease duration. *Mathematics.* 2022;10(15):2561. doi:10.3390/math10152561.
35. Shoaib Arif M, Raza A, Abodayeh K, Rafiq M, Bibi M, Nazeer A. A numerical efficient technique for the solution of susceptible infected recovered epidemic model. *Comput Model Eng Sci.* 2020;124(2):477–91. doi:10.32604/cmcs.2020.011121.
36. Abodayeh K, Raza A, Arif MS, Rafiq M, Bibi M, Mohsin M. Stochastic numerical analysis for impact of heavy alcohol consumption on transmission dynamics of gonorrhoea epidemic. *Comput Mater Contin.* 2020;62(3):1125–42. doi:10.32604/cmcs.2020.08885.
37. Shatanawi W, Raza A, Arif MS, Rafiq M, Abodayeh K, Bibi M. An effective numerical method for the solution of a stochastic coronavirus (2019-nCoV) pandemic model. *Comput Mater Contin.* 2021;66(2):1121–37. doi:10.32604/cmcs.2020.012070.
38. Saleem S, Rafiq M, Ahmed N, Arif MS, Raza A, Iqbal Z, et al. Fractional epidemic model of coronavirus disease with vaccination and crowding effects. *Sci Rep.* 2024;14(1):8157. doi:10.1038/s41598-024-58192-7.
39. Raza A, Baleanu D, Khan ZU, Mohsin M, Ahmed N, Rafiq M, et al. Stochastic analysis for the dynamics of a poliovirus epidemic model. *Comput Model Eng Sci.* 2023;136(1):257–75. doi:10.32604/cmcs.2023.023231.
40. Cheng X, Wang Y, Huang G. Global dynamics of a network-based SIQS epidemic model with nonmonotone incidence rate. *Chaos Solitons Fractals.* 2021;153:111502. doi:10.1016/j.chaos.2021.111502.
41. Khan IU, Mustafa S, Shokri A, Li S, Akgül A, Bariq A. The stability analysis of a nonlinear mathematical model for typhoid fever disease. *Sci Rep.* 2023;13(1):15284. doi:10.1038/s41598-023-42244-5.
42. Integrated Disease Surveillance & Response (IDSR) Report. Center of Disease Control, National Institute of Health, Islamabad; 2024. Available from: <https://nih.org.pk/idsr-weekly-bulletin>. [Accessed 2024].